Spatial Organization of Chromosomes in the Salivary Gland Nuclei of *Drosophila melanogaster*

Mark Hochstrasser, David Mathog, Yosef Gruenbaum, Harald Saumweber, and John W. Sedat

Department of Biochemistry and Biophysics, University of California, San Francisco, California 94143. Dr. Saumweber's present address is Max Planck Institut fur Entwicklungsbiologie, Spemannstrasse 35, 7460 Tubingen, West Germany.

Abstract. Using a computer-based system for model building and analysis, three-dimensional models of 24 *Drosophila melanogaster* salivary gland nuclei have been constructed from optically or physically sectioned glands, allowing several generalizations about chromosome folding and packaging in these nuclei. First and most surprising, the prominent coiling of the chromosomes is strongly chiral, with right-handed gyres predominating. Second, high frequency appositions between certain loci and the nuclear envelope appear almost exclusively at positions of intercalary heterochromatin; in addition, the chromocenter is always apposed to the envelope. Third, chromosomes are invariably separated into mutually exclusive spatial domains while usually extending across the nucleus in a polarized (Rabl) orientation. Fourth, the arms of each autosome are almost always juxtaposed, but no other relative arm positions are strongly favored. Finally, despite these nonrandom structural features, each chromosome is found to fold into a wide variety of different configurations. In addition, a set of nuclei has been analyzed in which the normally aggregrated centromeric regions of the chromosomes are located far apart from one another. These nuclei have the same architectural motifs seen in normal nuclei. This implies that such characteristics as separate chromosome domains and specific chromosome–nuclear envelope contacts are largely independent of the relative placement of the different chromosomes within the nucleus.

EUKARYOTIC cells contain enormous lengths of DNA that must undergo considerable packing to fit inside the interphase nucleus. The packing is accomplished through multiple foldings of the DNA molecule within each chromosome and the folding of the chromosomes themselves inside the nucleus. This hierarchy of foldings is under several general constraints. First, the DNA must be available to regulatory factors and transcriptional machinery in such a way that readout of the genome can be precisely controlled. Second, the resident copies of DNA must be faithfully duplicated and repackaged with histones and other proteins; in dividing cells, the daughter helices must also be topologically resolved. Finally, nuclear division depends on a number of tightly orchestrated events: condensation of chromatin into compact chromosomes, dissolution of the nuclear envelope, movement of chromosomes to a central plate with subsequent splitting of daughter chromatids toward opposite poles, decondensation of daughter chromosomes, and reassembly of the nuclear envelope around them.

Despite the interest in elucidating the means by which cells accommodate these constraints and package their genomes, only a meager sketch of higher order structures can currently be claimed. Beyond the level of the 10-nm nucleosomal fiber, little consensus has been reached. This is particularly true of the highest level of chromosome organization, the three-dimensional arrangement of chromosomes in the interphase nucleus. For reviews, see references 13 and 21.

The giant polytene nuclei of the *Drosophila* salivary gland provide a convenient model system for analyzing the folding patterns of interphase chromosomes by direct optical methods. These cells can be considered to be in interphase by several criteria (31). The basic question addressed in the present work is how a set of chromosomes, which are over 800 μm in total length and average 3–4 μm in width, is packaged within a nucleus that is some 30 μm in diameter. By studying this system with a combination of fluorescence optical sectioning microscopy, three-dimensional modeling, and quantitative analysis, we have been able to discover quite a number of consistent organizational motifs that characterize salivary gland nuclei in vivo.

This report represents a continuation of work begun several years ago (1), and a preliminary account of a portion of the current data was described previously (27). In the latter report, we drew several conclusions about the folding patterns of polytene chromosomes based on six nuclei from a single salivary gland. Four more nuclei in this gland were modeled and were discussed in a report on the spatial distribution of transcriptionally active sites (18). Here we discuss the results from a total of 24 reconstructed nuclei from 5 glands: 10 from the original gland analyzed, 7 from another gland of the same inbred stock that had been embedded in epoxy resin, and 7 from larvae of a different wild-type stock. The expansion of the data base as well as several additional methods of model analysis allow a number of new conclusions about nuclear

spatial organization to be made. Most of the present results are in general agreement with our preliminary reports, but several of the earlier interpretations had to be changed. A hierarchy of organization that includes features strictly conserved among the nuclei to aspects that are widely divergent is described.

Materials and Methods

Salivary Gland Samples

The method of sample preparation for optical sectioning was essentially the same as described by Mathog et al. (27). The buffers used in this study were buffer A (11) and the physiological buffer of Shield and Sang (37). Buffer A was made with either 15 mM Pipes or 15 mM Hepes, 0.15 mM spermine, 0.5 mM spermidine, 60 mM KCl, 15 mM NaCl, pH 7.4. The OR-isoX stock (obtained from S. Beckendorf) is a wild-type stock that has been made isogenic for the X chromosome. The other stock used is a highly inbred Oregon R stock.

The gland that had been embedded and sectioned was initially part of a uridine pulse-labeling experiment (18). Glands were dissected into Shield and Sang medium and, after the pulse-chase regimen, transferred to buffer A containing 3.7% formaldehyde (freshly prepared from paraformaldehyde [Kodak]). After fixing for 15 min, the glands were washed, stained with 3 μg/ml 4′,6-diamidino-2-phenylindole, and refixed for 60 min. After washing, the glands were stepped into dimethylsulfoxide, and finally embedded in Spurr epoxy resin (Polysciences, Inc., Warrington, PA). Polymerization was performed overnight at 65°C. Blocks were serially sectioned with a glass knife, and the 0.5-μm-thick sections were collected on coverslips. After mapping the location of well preserved nuclei, the sections were photographed on a Zeiss Axiomat microscope (Carl Zeiss, Inc., Thornwood, NY) using epifluorescence optics, the images being stored on a computer disk. Sections were aligned computationally (1).

For optical sectioning into the partially sectioned Spurr block, a special Plexiglas holder was made to hold the block on the stage of the Axiomat. A drop of oil was placed directly on the clean face of the block for use with a 100×/1.3 numerical aperture oil lens. 24 serial optical sections were taken for each nucleus using a step size of 1.3 μm, exactly as was done with glands observed in aqueous buffer.

To observe the salivary glands within the living animal, third instar larvae were washed in buffer and placed on clean slides; an 18 x 18-mm No. 1 coverslip was taped firmly over each while making sure the ventral aspect of the larva faced toward the coverslip. The larva cannot crawl away, and the obstructing fat body is often pushed out from between the salivary gland and the body wall, exposing the gland for viewing. A 100×/1.3 numerical aperture Planapo objective lens was used, and the field diaphragm was closed down almost completely. Banded chromosomes are readily followed under these conditions.

Microscopy and Model Building

The computer-controlled Zeiss Axiomat microscope for serial optical sectioning of polytene nuclei was as described (27, 29). Some hardware changes have been made. The Commodore Pet microcomputer (Commodore, Inc., Santa Clara, CA) that was used to control the focus stepping motor has been replaced by a Z8 microcontroller (Micromint, Cedarhurst, NY). The focus-stepping motor itself has been replaced by a microstepping motor (Compumotor). A lamp shutter, also controlled by the Z8, has been added to minimize unnecessary exposure of the sample.

The model building and analysis program IMP has also been delineated (27–29), although its capabilities have been expanded. None of the images from the aqueous samples were processed computationally. We found it helpful to apply Fourier filtering and out-of-focus removal algorithms to the blurrier images obtained from the optically sectioned embedded gland (details in reference 18).

Quantitative Analysis of Models

The histograms of triple product values (Fig. 3) were derived as follows. The model arm is divided into 512 evenly spaced points. Beginning at one end of the arm, a set of three consecutive vectors is placed on the model to connect points at 7-μm intervals. The triple product of their unit vectors, $T = \mathbf{A}\cdot(\mathbf{B} \times \mathbf{C})$, is then calculated (28). · is the inner product, × the cross product. The value is assigned to the midpoint of the model path between the outer ends of the three vectors, i.e., 10.5 μm from the model's end. The set of vectors is then shifted along the model path by one point, and the calculation is repeated. This entire procedure is continued until the leading end of the vectors reaches the other model endpoint. The range of triple product values so produced is then divided into 100 intervals, and the values are histogrammed. This was done in all 24 nuclei for each chromosome arm; each histogram in Fig. 3 thus represents the distribution of triple product values summed over 24 chromosome arms.

A point on a chromosome model that falls within 1 μm of the nuclear surface was defined as a nuclear envelope contact. To test the association between such contacts and loci containing intercalary heterochromatin, each chromosome was divided into intervals of three letter subdivisions (e.g., 12 A–C), and any interval in which the contact frequency (Fig. 5) was at or above the $P < 0.05$ cutoff (see Results) was counted in the tabulation. Only weak points present in at least 20% and ectopic fiber sites present in at least 15 out of 550 of the squashes of Zhimulev et al. (43) were counted as intercalary heterochromatin loci. The last four intervals (two divisions) closest to the chromocenter were not used. The χ^2 formula is

$$\chi^2 = n(ad - bc)^2/[(a + b)(a + c)(b + d)(c + d)],$$

where a is the number of intervals with both a high frequency contact and intercalary heterochromatin, b is the number of intervals with no contact but intercalary heterochromatin, c is the number of intervals with a contact but no intercalary heterochromatin, d is the number of intervals with no contacts and no intercalary heterochromatin, and n is $a + b + c + d$. The same statistic was used to evaluate the correlation between the high frequency surface contacts in the different contributing data sets used in this study. In these cases, a 0.5-μm limit was used to generate the frequency plots. The frequency cutoffs for the different sets were as follows: nuclei with split chromocenters (see Results), 4–5 out of 5; nuclei from the embedded gland, 5–7 out of 7; and nuclei from the original unfixed gland, 7–10 out of 10.

The Monte Carlo procedure used to estimate the random probability distribution for surface contact frequencies for a chromosome arm works as follows. Distance-to-surface plots, which plot the minimum distance between each cytological position and the nuclear surface versus cytological position (e.g., Fig. 6, in reference 27), provide the set of input distance values. One distance value is randomly chosen from each of the 24 plots for a chromosome arm. The 24 selected values are then compared with the cutoff value of 1 μm used to generate the surface contact frequency plots, and the number of values less than or equal to the cutoff is counted. This entire procedure is reiterated 10^6 times. The final result is a tabulation of the frequencies with which 0, 1, ... 24 out of 24 randomly selected values fell within the cutoff distance.

Chromosome intradistance plots (Fig. 7) were generated as described previously (27). To generate a set of control intradistance plots with intradistance values randomly displaced with respect to position on the chromosome, the values in each of the original plots were shifted by a random amount in a direction along the diagonal (see Fig. 7); the magnitude of the shift is different for each plot. The shift causes a portion of the distance values to roll off the right side of the plot; this is then patched back onto the bottom. The entire transformation can be visualized as follows (see Diagram I). An isosceles right triangle placed on its side (intradistance plot), originally superimposed over a second (*1*), is displaced by some amount along the diagonal (*2*). The region of overhang where the top triangle no longer overlaps the other (indicated by cross-hatching) is cut off and pasted to the exposed portion of the bottom triangle. This involves a 90° counterclockwise rotation in the plane of the paper and a reflection across the x-axis. This method introduces a discontinuity at the border of the patch but retains all the distance information from the original plot; moreover, the displaced intradistance values remain at their original distances from the diagonal despite being in new places with respect to cytological position (this is illustrated by the shaded section in the diagram). The mean and standard deviation of the randomly superimposed distance values at each point are then calculated as before.

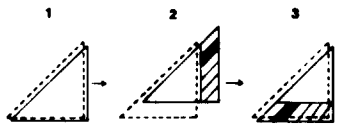

Diagram I

Results

The approach we have taken to describe the spatial arrangement of chromosomes is direct and in principle quite simple. The specimen is stained with a DNA-specific fluorescent dye and prepared for microscopy. Fluorescence images from serial

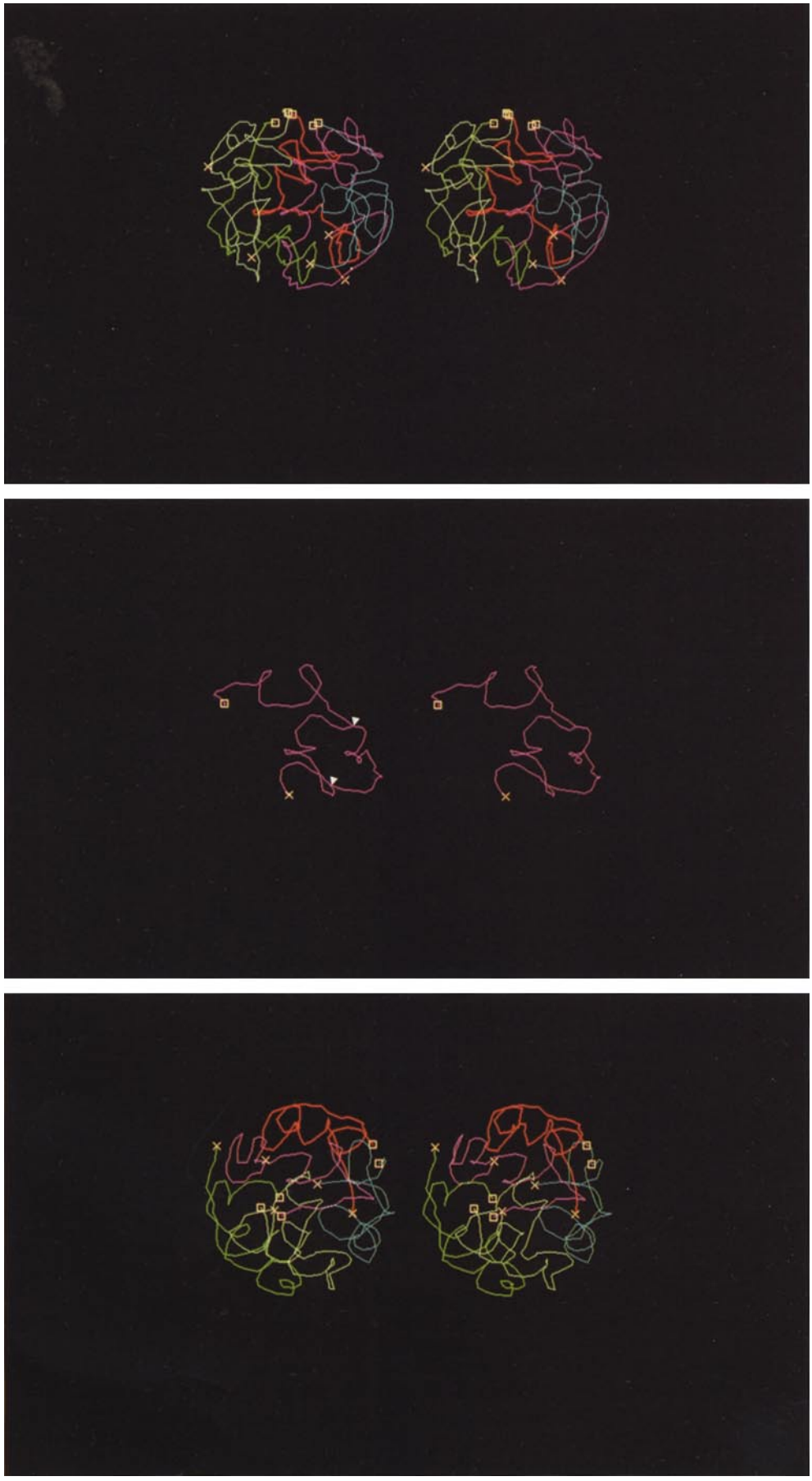

sections of nuclei are collected, and from such image stacks, the paths of the five major chromosome arms are traced using an interactive modeling program (27–29). Subsequently, quantitative properties of the resulting stick figure models are measured and displayed. The models and quantitation plots are used to derive a detailed structural description of chromosome folding. Details of methodology are published elsewhere (27–29), and any modifications are noted under Materials and Methods.

Orderly Large Scale Organization of Chromosomes

Several general organizational features discovered by Mathog et al. (27) by inspecting stereo-pair models of nuclei have been further documented in the present study. First, the chromosome arms are always maintained in separate spatial domains within the nucleus, with no arm looping around another even though the chromosomes are highly contorted and closely packed (Figs. 1 and 8). Second, the centromeric regions of salivary gland chromosomes, which are usually aggregated together to form an amorphous mass called the chromocenter, are always positioned against the nuclear envelope. Such an invariant association between centric heterochromatin and the nuclear envelope recalls a similar situation documented in *Drosophila* early embryos (14; Sedat, J. W., unpublished observations). In early embryos the chromocenter is always at the edge of the nucleus closest to the topological exterior of the embryo. In contrast, the chromocenter in salivary gland nuclei is found in a wide range of positions relative to the gland lumen; our earlier inference of a very limited range (27) is therefore not generally true. Finally, a related motif of chromosome organization that is observed is the Rabl orientation (15, 35; Fig. 1). This is the grouping of centromeres near one pole of the nucleus with the telomeres arrayed in the opposite hemisphere. 80% of the chromosome arms have configurations that fulfill this criterion.

Preferred Relative Arrangements of Chromosome Arms

Considerable effort has been directed toward determining whether there are any favored relative arrangements of chromosomes within the nucleus (4). Perhaps the best evidence for nonrandom chromosome positions has been reported by Bennett (8), who looked at centromere positions in thin-sectioned mitotic plant cells. Coates and Smith (12), however, using the same method of analysis as Bennett, came to the opposite conclusion for hybrid grasshopper cells. We find that the relative arrangement of the major chromosome arms in salivary gland nuclei is not entirely arbitrary. Because the bulk of each arm is generally situated between only two neighboring arms and the arms lie in noninterwoven domains (analogous to the sections of a grapefruit), it is usually straightforward to determine their relative arrangement. Fig. 2 shows the different arrangements in schematic fashion; in one of the nuclei the relationships cannot be uniquely assigned and are therefore not included. As can be seen, 2L and 2R are almost always next to each other; the same is true for 3L and 3R (21/23 in both cases). Besides these, the strongest preference for particular arrangements of arms is seen if one groups the nuclei according to whether the right arms of the autosomes and/or the left arms are next to each other (*cis*) or are in the complementary arrangement (*trans*). The *cis* constellation is seen more than twice as often as the *trans*. It remains possible, however, that this is a sampling effect; even if a 1:1 ratio of these two types actually exists, such a bias in a sample of this size is not significant ($\chi^2 = 1.45$, $P > 0.20$). Other small biases in the relative frequencies of nearest neighbor pairs pointed out previously (27) may also have been due to sampling. The X chromosome, for example, while almost always between the two autosomes, is not preferentially positioned next to any particular arm. In only one nucleus were the arms from autosomes 2 and 3 interdigitated (but not entangled).

Relative positions of chromosome arms can be assessed in several additional ways. One is to calculate the center of mass of each arm and measure the distances between them. Another is to look at the interdistance maps for each pair of arms in each nucleus and find which pairs have the highest number of close sites. Both methods yield the same qualitative conclusions just described (data not shown). Thus, it appears that the arms of each autosome remain close together in the nucleus, whereas other relative arm positions vary considerably.

Chromosome Coils Are Right-Handed

It is evident from the models (Figs. 1 and 8) that a dominant folding motif of the salivary gland chromosome is the coil. What is more striking, however, is that these coils almost always appear to be right-handed (see also Fig. 3 in references 18 and 27). This is a surprising result as no such chirality has previously been reported either in mitotic or polytene chromosome coiling (7, 26). To demonstrate the asymmetry by an independent and more quantitative method, we have used the triple product, a standard vector operation, which has been used previously to analyze helices in proteins (9). The triple product, $\mathbf{A}\cdot(\mathbf{B}\times\mathbf{C})$, where **A**, **B**, and **C** are successive vectors along a path, yields a scalar value whose sign depends on whether the vectors' relative orientations in space follow a left- or right-handed screw. A positive value indicates a right-handed screw, a negative value a left-handed one. Here we

Figure 1. A stereo pair model of a salivary gland nucleus. The figure shows the generally polarized orientations of chromosomes (3R is an exception) and the absence of any intertwining between arms. Chromocentral endpoints for each arm are marked with squares; telomeres are indicated with crosses. Note that the proximal heterochromatic portions of the arms that form the chromocenter are not modeled, so the arms of each chromosome are not connected. The color code of the arms is: X, green; 2L, red; 2R, blue; 3L, purple; 3R, light green. The diameter of the model is ~32 μm.

Figure 4. Asynapsed 3L chromosome arm. The region of asynapsis extends from ~63A–69A (endpoints marked with arrowheads). Right-handed coils are evident in both the synapsed and asynapsed portions of the arm, the latter having smaller radii. The scale is the same as in Fig. 1. The proximal endpoint is marked with a square, the telomere with a cross.

Figure 8. A stereo pair model from a nucleus with a split chromocenter. The two chromocenters are ~20-μm apart. Chromocentral endpoints for each arm are marked with squares; telomeres are indicated with crosses. Chromosomes 3 and X are attached to one chromocenter, while chromosome 2 is at the other. The color code and scale are as in Fig. 1.

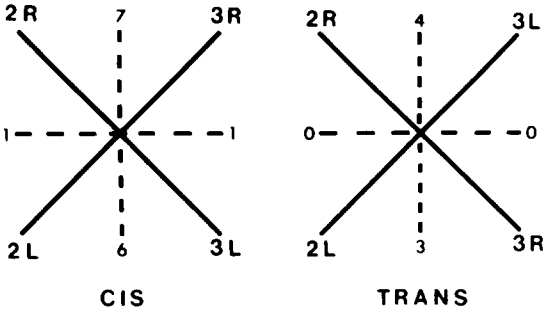

Figure 2. Relative arrangements of chromosome arms. In one nucleus relative arm positions cannot be assigned uniquely and so cannot be included in the figure. In another nucleus the arms from the different autosomes are interdigitated, and it is omitted here for clarity. 15 of the remaining 22 nuclei are in the *cis* arrangement, 7 in the *trans* (see text for definitions). The various positions of the X chromosome are shown with dashed lines. The number of nuclei in which it is in each position is noted.

use a set of three unit vectors connecting points located at 7-μm intervals along the model arm. The set of vectors is slid along the model path and their triple product is calculated at each of 512 equally spaced points (28; Materials and Methods). Fig. 3 displays histograms of the triple product values for the five major arms gathered from all 24 nuclei; zero is at the center. The distributions are all strongly skewed to the right, with the ratio of positive to negative values ranging from 2.0 to 2.7. This demonstrates that the direction of coiling along each chromosome is indeed predominantly right-handed.

Two comments need to be made about these plots. First, the selection of a particular vector size acts as a filter for curves in that size range. Vectors spaced at 7-μm intervals were chosen because the patent coils seen in the models are some 15–30-μm long; this set of three vectors samples the pathway in the desired range (3×7 μm = 21 μm). Use of other sizes, however, yields qualitatively similar plots as long as they are not extremely small or large. Second, there are certainly segments of some chromosomes that are not particularly coiled. These, along with coils of little or no pitch, will contribute to a set of triple-product values at or close to zero; also, although almost no clearly coiled regions are left-handed, some stretches, especially around sharp bends, do yield negative triple product values.

Preliminary evidence suggests that a chromosomal region need not be homologously paired for it to display a right-handed chirality. We have found an example (Fig. 4) of a 3L chromosome arm that has an asynapsed region stretching from about 63A to 69A, over a third of the arm's length. The coils in the thinner, unpaired homologs are smaller than in the synapsed regions, but they are still right-handed. This is confirmed in their respective triple product plots (not shown).

A Set of Loci Regularly Contacts the Envelope

Previously, we tabulated a set of loci that were almost always positioned against the nuclear envelope in the six nuclei examined (27). Now, having 24 reconstructed nuclei from five larvae of two different stocks, we can make a statistically more meaningful statement about which loci are frequent surface-contacting sites. The individual data sets were first examined separately. We observed a certain amount of variation between them which may be stock or larva specific; for

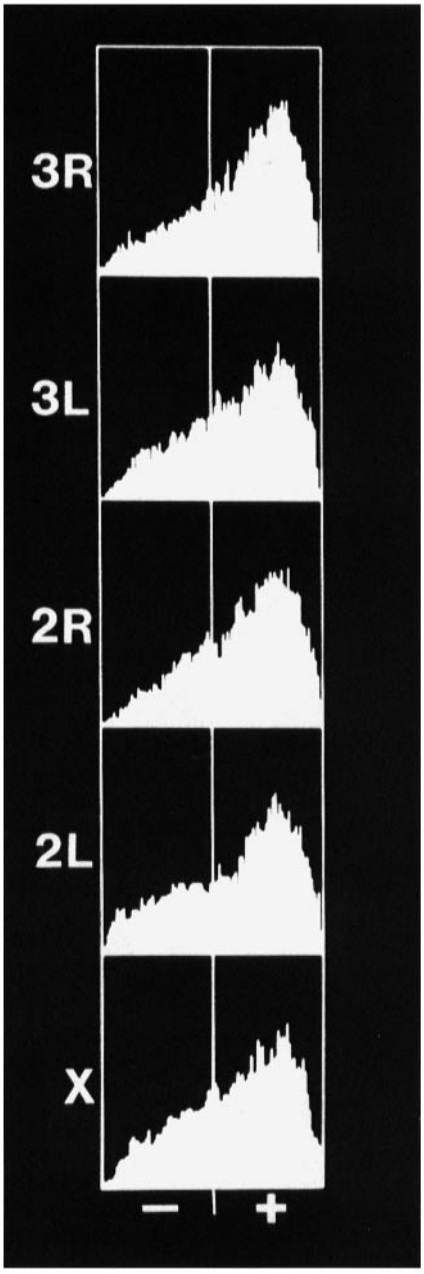

Figure 3. Triple product value histograms for each major arm. Values are summed from 24 nuclei. See text for details. The vertical scale is arbitrary. The center line in each histogram is at the point of zero handedness, i.e., the triple product value equals zero. All values to the right of this line are positive and indicate right-handedness, and the opposite is true of those values to the left of it. The ratios of positive to negative values using a 7-μm spacing between unit vectors are: *X* (2.0), *2L* (2.0), *2R* (2.5), *3L* (2.2), and *3R* (2.7). To avoid end effects when calculating the triple products, the calculation is terminated when any of the vectors reaches an end of the chromosome path.

example, the 5F/6A site is on the surface in 10 out of 10 nuclei in the original gland but is rarely there in all the other nuclei examined. However, the majority of high frequency surface contact loci are the same among the different sets of nuclei (see below). While the variations may have significance, we do not yet have enough data to evaluate them properly. Consequently, we have pooled the surface contact frequencies

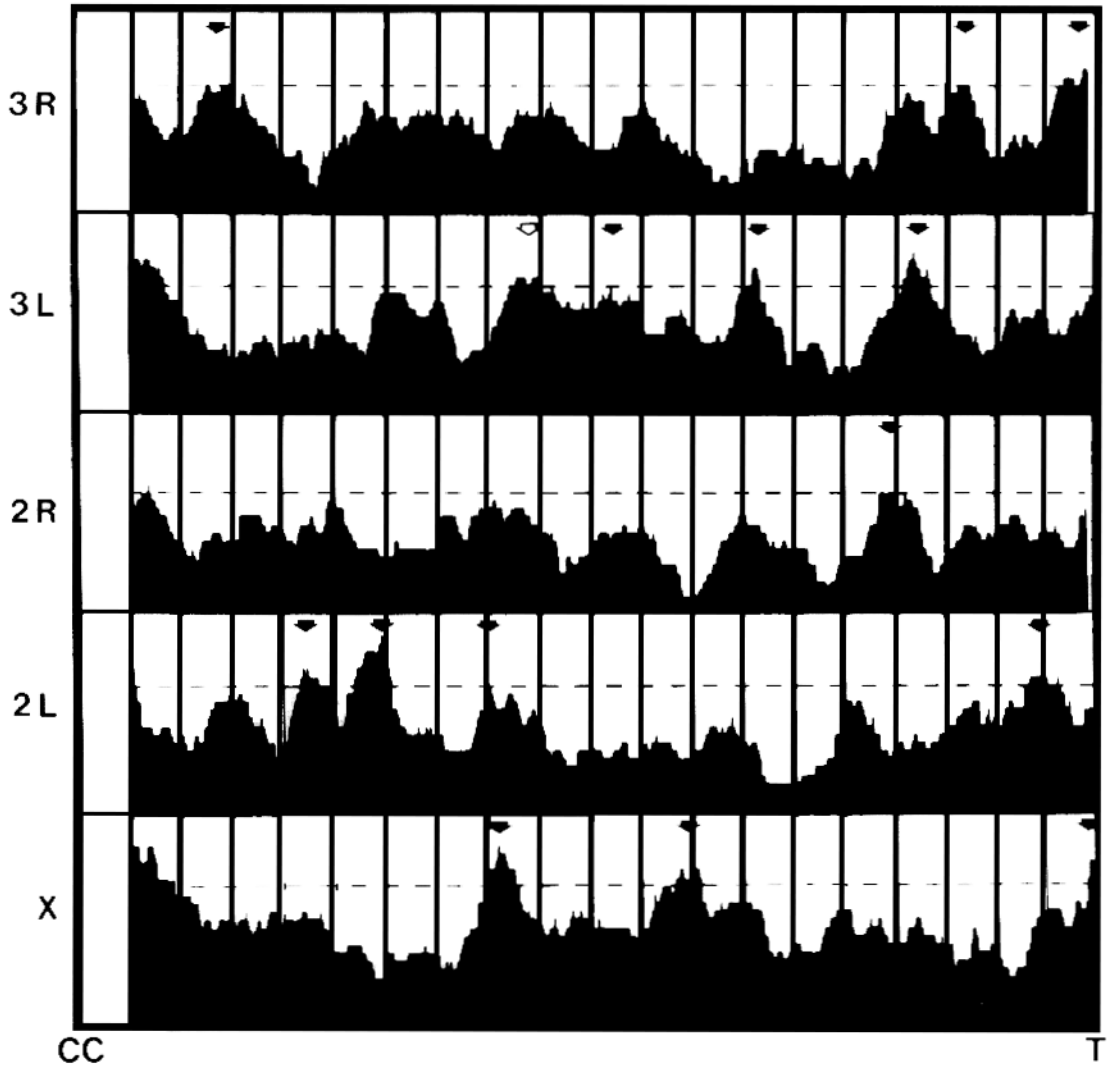

Figure 5. Nuclear surface contact frequencies for the five major chromosome arms. A locus is regarded as on the nuclear envelope if it is within 1 μm of the surface. The nuclear surface is approximated by a convex polygon in which the model is inscribed (27). Cytological position is plotted along the abscissas of each plot, the chromocenter (*CC*) on the left, the telomere (*T*) on the right. The ordinate range is 0–24 (out of 24). Each horizontal division represents one cytological division (e.g., 1A–1F) in the respective arms (10, 24). The values in the left-most division in each plot have been set to zero because the cytology is never followed into these regions. The data in the second division from the left of each arm is displayed but is not included in the analysis because cytological identification is sometimes difficult close to the chromocenter. The telomeres in the 2R and 3R plots fall one letter subdivision short of the right end, so the rightmost ends in these two plots are set to zero. The average fractions of each model arm within 1 μm of the surface are approximately as follows: *X* (0.46), *2L* (0.46), *2R* (0.40), *3L* (0.47), *3R* (0.42). The arrows highlight regions where the frequency of contact is at or above the cutoff frequency for the arm (indicated by the dashed line). The cutoffs used are as follows: *X* (16 out of 24), *2L* (16), *2R* (15), *3L* (16), *3R* (15). Approximately 8% of each arm's plot is at or above the cutoff. The dark arrows indicate an overlap with a position of intercalary heterochromatin, while the open one means no intercalary heterochromatin is in that contact region.

for all 24 nuclei, thereby concentrating on the contacts preserved in all data sets.

Pooled envelope contact frequencies for the 5 major arms are shown in Fig. 5. Each arm is divided into 512 evenly spaced points; when a point falls within 1 μm of the nuclear surface, the point is counted as a contact site. As described previously (27), cytological bands on the chromosomes are identified and used as fiducial marks when comparing the same chromosome in different nuclei. The frequency with which a locus apposes the nuclear envelope in this set of nuclei varies markedly along the length of each chromosome arm. Some regions are on the surface in almost every nucleus examined, others in a majority of cases. However, to judge the significance of the frequency peaks (and valleys) it is necessary to determine how often one would observe such frequencies if surface-contacting regions were located randomly on each chromosome arm. Rather than assume a particular type of random frequency distribution, a Monte Carlo procedure was used to generate one from the input data so that the random distribution would match the real data in the percentage of the arm in each nucleus that was in contact with the surface. The procedure is described in Materials and Methods.

All frequency peaks whose probability of occurring randomly is <0.05 (probability of occurring this many or more times) are marked with arrows in the plots. This cutoff is

somewhat arbitrary. It was chosen so that only peaks with a relatively low probability of representing random juxtaposition would be considered, but it is not low enough to eliminate this possibility. By this criterion, at least 15 loci along the chromosomes are on the nuclear envelope with frequencies that are unlikely if contacts were only made randomly (see figure legend). However, additional information is needed to verify whether the indicated peaks are specific for particular chromosomal loci.

We searched the literature for evidence of any structural peculiarities common to these loci (27). A comparison of our persistent envelope contacts to the positions of intercalary heterochromatin mapped by Zhimulev et al. (43) reveals a very strong correlation between the two. Intercalary heterochromatin is a term for sites along the chromosomes with properties typical of centric heterochromatin from either polytene or diploid cells. These include frequent ectopic fibers, constrictions in polytene squash preparations, late replication, frequent breakage from irradiation, and certain chemical (5) and genetic properties (40).

In Fig. 5, 14 of the 15 regions marked with arrows are centered on loci that show frequent ectopic pairing and/or weak point behavior, two of the most stringent criteria for the presence of intercalary heterochromatin. The degree of association was evaluated from a 2 × 2 contingency table with a chi-square statistic and was found to be highly significant ($\chi^2 = 23.7$, $P \ll 0.001$; see Materials and Methods). An examination of intercalary heterochromatin sites in section images suggests this correlation may indeed be relevant (Fig. 6). These sections show intercalary heterochromatin bands that appear to be pulled out toward the nuclear surface, suggesting a physical connection. A section with chromocenter material pressed against the surface is also shown. To summarize, three sets of observations argue that specific loci are involved in frequent chromosome–envelope interactions: (*a*) a set of loci are on the surface with high frequency, (*b*) almost all of these loci coincide with intercalary heterochromatin positions, and (*c*) these sites often appear in physical sections to be attached to the surface. It should be noted that although some of the lowest dips in Fig. 5 are as statistically unlikely as some of the peaks, there is no correlation with intercalary heterochromatin ($\chi^2 = 1.68$, $P > 0.10$), again using a $P < 0.05$ cutoff; we have not yet found any other structural correlates to these sites, so their biological significance remains unknown.

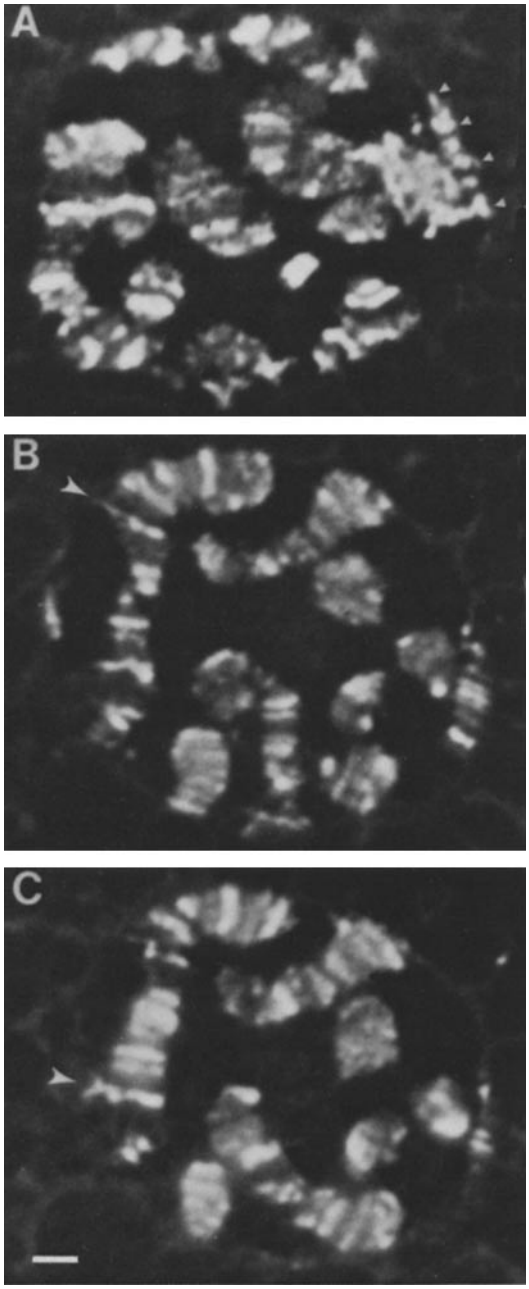

Figure 6. Physical sections of 4′,6-diamidino-2-phenylindole-stained salivary gland nuclei. (*A*) Example of chromocenter material appressed to the nuclear surface (arrowheads). (*B*) A locus containing intercalary heterochromatin, 70C, apparently attached to the nuclear surface (arrowhead). (*C*) Another intercalary heterochromatin site, 71C, showing an apparent attachment (arrowhead). Sections *B* and *C* show the same 3L chromosome arm in successive 0.5-μm sections. Bar, 2 μm. The cytoplasm fluoresces weakly in the embedded gland, so the nuclear border can be seen in the sections. To accentuate the cytoplasmic staining for display purposes, the section images were processed with a program that compresses the overall dynamic range in the image while providing local contrast enhancement (written by Andrew Belmont).

Chromosomes Assume a Wide Variety of Configurations

Several studies have shown a restricted spatial distribution of certain DNA sequences in the nucleus (20, 25). Some authors have suggested that the configurations of chromosomes within the interphase nucleus are under specific genetic control (41, 42). In a direct approach to these problems, we have been analyzing chromosome folding patterns with the aid of intradistance plots (27, 36). For such plots, the absolute distances between all pairs of points on a chromosome model are measured (the model path is traced through the approximate center of the 3–4-μm-thick arm) and then plotted on a two-dimensional map in which each axis represents cytological position along the arm. The pattern of intensity values is therefore a mapped representation of the three-dimensional folding of the chromosome.

Fig. 7*A* shows a sample intradistance plot of chromosome arm 2L from one nucleus. The contoured set of distances are displayed as intensity values, the darkest regions representing pairs of chromosome points that are closest together in space. Contour steps are 2 μm, and intradistance values larger than

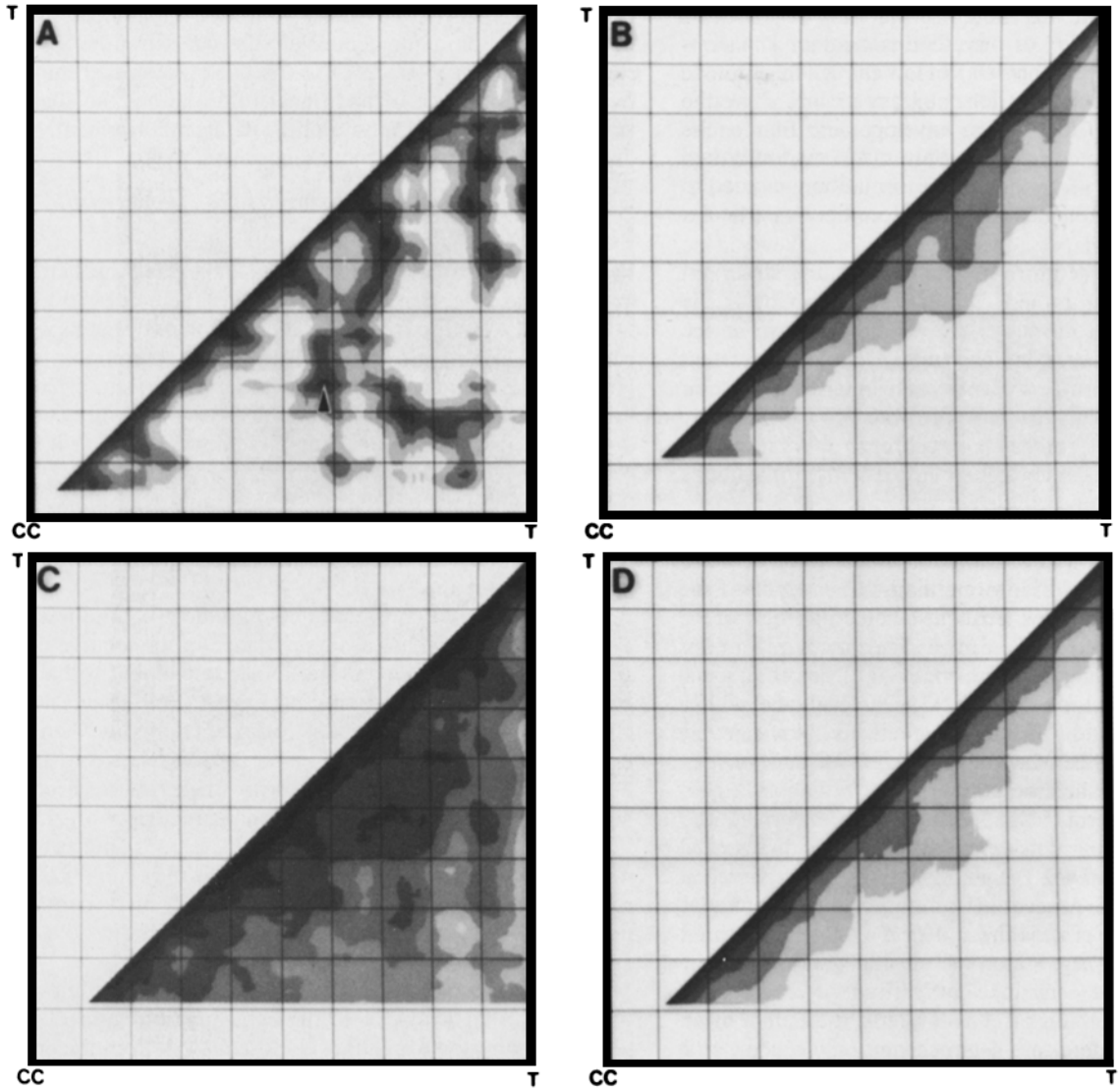

Figure 7. The three-dimensional folding of chromosome arm 2L. (*A*) A contoured intradistance plot for one 2L arm. See text for derivation. Cytological position is plotted along both abscissa and ordinate with grid lines separated by two cytological divisions. The telomere (T = 21A) and the chromocentral endpoint (CC = 40F) are marked (the plot is actually never interpolated beyond 40A). The average length of the 2L model arm is 146 μm. The darkest regions mark pairs of loci closest together in space. Contour steps equal 2 μm. All distances greater than 10 μm are displayed as white. The arrowhead points to an apposition between 29B and 35E in the model; their separation is between 2 and 4 μm. (*B*) The mean intradistance plot for 2L (24 nuclei). The value at each point represents the mean distance between the pair of loci denoted by that point. Values are plotted as in *A*. The bottom portion of the plot is truncated because the chromosome banding pattern could not be traced in every nucleus into this proximal region of the arm. (*C*) The standard deviation map for 2L. The value at each point represents the standard deviation of the distribution of distances between the pair of loci denoted by that point. The darkest values have the lowest standard deviations (<1 μm); contour steps in this plot are at 1-μm intervals. (*D*) The mean intradistance plot for the set of 24 2L intradistance plots that had been randomly displaced relative to one another. The plot is displayed exactly as in *B*.

10 μm are not displayed. This representation of the arm's configuration reveals a variety of appositions between loci. When such maps are compared for the same chromosome in different nuclei, common contacts and configurations should be apparent if they are present.

One way to compare all the nuclei with a data set of this size is to generate a mean intradistance plot. Such a plot is shown in Fig. 7*B* for chromosome 2L that is derived from the 24 individual 2L intradistance plots. Loci that are consistently paired in the different nuclei would appear as dark areas off the diagonal. In none of the mean plots for the five major arms are such areas present. When the standard deviations of the intradistance values between each pair of loci are plotted in a two-dimensional map (Fig. 7*C*), they show a general increase with distance from the diagonal. In fact, they increase roughly linearly with the corresponding mean intradistance values, although several areas in Fig. 7*C* show small standard deviations in places where the mean values are relatively high.

These plots therefore appear to provide little evidence of closely circumscribed three-dimensional chromosome configurations. This view is strengthened by the following control experiment. As described in Materials and Methods, intradistance values were randomly displaced relative to cytologi-

cal position by a different amount in each of the 24 plots, and these randomly shifted plots were then compared. The shifts scramble the distance information, and the resulting mean and standard deviation plots reflect only the random overlap of the original plots' features. The resulting mean plot for the randomly shifted data is shown in Fig. 7*D*. The similarity to Fig. 7*B* is striking: regular contacts are limited to regions close to the diagonal, and mean intradistances increase at a similar rate with distance from the diagonal. Likewise, the standard deviation plot for the randomized data is also qualitatively very similar to Fig. 7*C*, with standard deviation values increasing no more rapidly with distance from the diagonal and with several regions of low standard deviation off the diagonal (plot not shown). The simplest explanation for these results is that the observed interactions primarily reflect the confinement of the chromosome to a very restricted volume with no requirement for specific pairwise interactions between loci (see below).

It could be argued that several different well defined sets of interactions are present in the different nuclei, but by considering them all together this information is obscured. The issue has been tested in two ways. First, we studied printouts of the 24 individual 2L plots and attempted to sort them into groups according to shared folding features using their off-diagonal patterns of intensity (e.g., Fig. 7*A*). No two plots exhibit a similar set of off-diagonal contacts, so no two 2L chromosome arms can have very similar longer range interactions (i.e., interactions between loci separated by more than 1–2 cytological divisions). Second, the 24 plots were transformed into a set of 24 rank order plots (27). The values that are ranked in ascending order are the 24 intradistance values recorded at each pixel. Thus, the original plots are reorganized into a set in which each pixel in the rank = 1 plot contains the lowest intensity value (closest contact) recorded at that pixel in the original set of plots, each pixel in the rank = 24 plot the highest. For instance, if a pixel in the rank = 12 plot has an intensity corresponding to a 5-μm separation, then the pair of loci denoted by that pixel are within 5 μm of each other in at least 12 of the 24 nuclei.

The off-diagonal features rapidly disappear as one goes up in rank (data not shown). By rank = 6, 36D–38C are the only loci separated by more than about one cytological division (~7–8 μm) that are within 4 μm of each other. That is, no pair of widely spaced loci besides this one is closely apposed in even one fourth of the nuclei. No model sites separated by more than one cytological division come within even 5 μm of one another in 12 or more nuclei. So although there may be some similarities in the local bending of the arm in some of the nuclei, there is little support for a unique or small number of similar longer-range configurations. These results argue that the variation seen in the pooled data cannot be explained simply by positing the existence of a small number (say, 2–3) of classes of nuclei with different but uniform chromosome folding patterns.

That contacts between loci are generally not specific is further supported by performing the same ranking operation on the 24 randomly shifted intradistance plots described above. When the real and the randomized data are compared, it is found that the off-diagonal features disappear just as quickly in both as one goes up in rank (data not shown). The ranked features are also similar in shape and distribution, suggesting that in both cases they arise from the chance overlap of intensities. It therefore appears that no longer-range chromosome interactions are the same in more than a small number (at most 25%) of the nuclei examined; moreover, in the absence of additional information, the shared contacts in such small subsets of the data cannot presently be distinguished from random juxtapositions.

Chromosomes Packaged Similarly in Nuclei with Split Chromocenters

From the reconstructions of several salivary gland nuclei from another wild type stock of Oregon R flies (here referred to as OR-isoX), it was discovered that the centromeric regions were occasionally split into two well separated chromocenters. Hence, they cannot be organized in the usual Rabl orientation. Such separation of the normally fused centromeric sequences seems to occur in a small fraction of nuclei as it has been observed now in a number of larvae. Both Appels et al. (2) and Hammond and Laird (20) have reported examples of salivary gland nuclei with two separate hybridization sites to a chromocenter-specific DNA probe, so the phenomenon may not be uncommon.

Nuclei with split chromocenters provide a natural test for the question of whether a major change in the relative positions of portions of the chromosome complement will affect other aspects of chromosome packaging. For instance, are chromosomes still kept in spatially distinct domains when the orientation of some of the arms is flipped relative to their neighbors? Two OR-isoX nuclei with single, intact chromocenters have been modeled and exhibit the same organizational motifs discussed above (nuclear envelope contacts were not evaluated since with only two nuclei, they could not be reliably analyzed). Hence, any differences observed in the nuclei with split chromocenters should not be due to stock variations.

We have been able to find five nuclei with split chromocenters to date. In 4 out of 5, the centromeric region of the second chromosome is found 15–30 μm away from the other chromocenter; in the fifth, chromosome 3 is split off. Fig. 8 is an example of a nucleus in which separate chromocenters are on almost opposite sides of the nucleus (a neighboring nucleus shows a similar large split). Despite the reconfiguration, all chromocenters are still apposed to the nuclear envelope, the arms remain in domains, chromosomes coil into right-handed gyres, the arms of each autosome are usually close together, and most of the high frequency nuclear envelope contacts are the same. This last conclusion follows from a comparison with the 10 nuclei from the original gland; the correlation of high frequency contacts between the two data sets was evaluated from a 2×2 table as above and was shown to be statistically significant ($\chi^2 = 4.97$, $P < 0.05$; see Materials and Methods). As might be expected from the results presented above, the high frequency contacts in the nuclei with split chromocenters are also associated with intercalary heterochromatin loci ($\chi^2 = 8.44$, $P < 0.01$).

Different Preparative Procedures Do Not Alter Organizational Rules

The gland yielding the first set of ten reconstructions and the OR-isoX glands were all viewed in an aqueous buffer optimized for chromosome structure preservation (buffer A) and were not fixed. However, the organizational rules described are independent of the preparative procedures used. A very

different procedure was used for comparison (18; Materials and Methods). Glands from a late third-instar larva of the inbred wild-type stock were fixed, dehydrated, and embedded in Spurr's resin. After collecting a set of serial physical sections, optical section data were obtained from the unsectioned remainder of the embedded gland by focusing into the block. Two nuclei were reconstructed from aligned physical sections, five from the optically sectioned block. The glands were estimated to be in puffing stage (PS) 5–6 (3); the glands in the other data sets were in PS 7–8.

The nuclei show all of the structural features exhibited by the other sets of nuclei (data included above). The high frequency contacts are similar to those in the original unfixed gland of the same stock ($\chi^2 = 5.48$; $P < 0.02$), and correlate strongly to intercalary heterochromatin loci ($\chi^2 = 9.98$, $P < 0.01$). Thus, the structural motifs we could observe in the unfixed, minimally processed glands are maintained in embedded and physically sectioned nuclei, even though the glands are slightly different in developmental (i.e., puffing) stage. These results and those of the previous section provide the justification for considering all 24 nuclei from a total of five female larvae together in the preceding results.

Controls

Although the aim of the present work was to determine the in vivo folding of salivary gland chromosomes, the glands were not actually observed in vivo, strictly speaking. It is therefore necessary to show that the chromosomes do not rearrange appreciably as a result of our manipulations. To this end, several control experiments were performed. First, the same nucleus was optically sectioned at both the beginning and the end of a data-collecting session, and the two data stacks were compared by visual inspection. No differences were noted. Second, glands were dissected into buffer A or physiological buffer and immediately mounted for viewing with bright field optics. The banded chromosomes are easily discerned under these conditions, and any movement over a time period of minutes to hours would be detected. None was.

Our analysis is also based on the assumption that chromosome positions are relatively stable when the glands are in their normal milieu. To test this, salivary gland nuclei were viewed directly through the ventral body wall of living third instar larvae that had been immobilized between a coverslip and slide. Active movements within the body cavity continue, but it is not difficult to track particular banded regions in a single nucleus for several hours and thereby examine the relative positions and orientations of chromosome segments. No obvious repositioning of any chromosome region within the nucleus until histolysis was detected. During this latter period, cells become increasingly vacuolated and the chromosomes then do shift appreciably. Hence, since the glands we have examined are not histolysing, we are confident that our data describe the authentic in vivo configurations of chromosomes.

Discussion

We have described a number of regular motifs that characterize the organization of salivary gland nuclei. They include: invariant association between the chromocenter and nuclear envelope, confinement of the arms to non-intertwined spatial domains, certain nonrandom relative chromosome arm positions, Rabl orientation of chromosomes, envelope contacts that are locus specific and correlate with intercalary heterochromatin, and a large predominance of right-handed chromosome gyres. On the other hand, chromosomes fold into a wide variety of configurations that bear few obvious similarities between nuclei. Moreover, a gross relative repositioning of a portion of the genome in nuclei with split chromocenters does not alter any of the above motifs (except the Rabl orientation). In sum, a scheme of chromosome packaging can be described that contains both well ordered and apparently indeterminate features.

To interpret our results, it is useful to seek parallels with the organization of diploid nuclei. In what follows, much of the present data is rationalized through a consideration of the origin of the salivary gland as a diploid rudiment in the early embryo (38). This interpretation implies a high degree of positional stability of interphase chromosomes since many days have passed between the final embryonic mitosis and the stage at which we examine the gland. This is especially striking when one considers that in the intervening period the nuclei have increased in volume several hundred-fold and undergone 9–10 additional rounds of DNA replication. A stable intranuclear chromosome topology has been inferred from a number of different studies with diploid cells (22, 39, 44). Moreover, the retention of similar relative positions of chromosomes through an entire cell cycle has also been seen (32). We also know from our control experiments that at least in the last hours of third instar, salivary gland chromosomes are likely to be immobile.

The Rabl orientation has been repeatedly documented in diploid cells (13, 15, 16), where it is regarded as a relic of mitosis. It seems unlikely that it has a completely different cause in polytene tissues. The fact that the arms of each autosome are almost always close together (Fig. 2) is also consonant with the retention of telophase chromosome positions during polytene interphase.

Normal telophase chromosomes are dense structures that are topologically separable from one another. It is tempting to view the nonintertwined chromosome arm domains in third instar salivary gland nuclei as a vestige of this mitotic condition. In other words, as the cell progresses into interphase, the unraveling of each chromosome takes place entirely within the boundaries presented by neighboring chromosomes and the nuclear envelope. Indeed, the orderly condensation and division of chromosomes in mitotic cells supply a possible rationale for maintaining stable, noninterwoven domains during interphase. *Drosophila* chromosomes must nevertheless find and synapse with their homologs since it is known from neuronal cells and cell culture lines that during metaphase and anaphase, homologs are not tightly paired (6, 19); this requires local chromosome movement and fusion of homolog domains. A striking example of the strength of these pairing interactions comes from flies heterozygous for a whole X chromosome inversion; after completing mitosis with the centromeres of the two homologs aligned, a complete reorientation of one homolog relative to the other occurs, allowing the two to synapse (6).

The surface contact data (Fig. 5) reveal a number of preferred associations between the chromosomes and nuclear envelope. There are, however, additional peaks in the plots that fall below our statistical cutoff which may also be specif-

ically positioned at or interacting with the nuclear surface. For example, a smaller peak is observed at 25EF on 2L that coincides exactly with an intercalary heterochromatin site. However, we can only discuss with confidence loci that have a very strong propensity for making nuclear envelope contacts. Possibly, an intercalary heterochromatin locus's position within a chromosome may modulate its ability to reach the surface; small translocations that move a surface contacting locus to new positions should help answer this question. Finally, groups of individual distance-to-surface plots from different nuclei sometimes look quite similar over considerable stretches (see Fig. 6 in reference 27), and we are currently examining whether this can be interpreted in terms of discrete, alternate chromosome attachment patterns.

A plausible way to view these results is that as a cell emerges from mitosis, a large number of chance contacts with the nascent envelope occur, with a subset of loci making more stable associations. As the nucleus progresses into interphase, these associations tend to persist. It is also possible that the high frequency contact loci represent preferred nucleation sites for envelope reformation. The correlation of the contacts with intercalary heterochromatin suggests that the heterochromatic nature of these loci allows them to bind more tenaciously than other loci to envelope structures and may account for the selectivity. Such a contention is supported by the data in Fig. 6 as well the micrographs of Quick (34) and Gay (17), showing the adhesion of ectopic fibers or dense heterochromatic material to the nuclear envelope. The idea that nuclear envelope attachments are established relatively early in salivary gland development is lent credence by the fact that heterochromatic material is known to bind to the nuclear envelope in diploid nuclei (13). This may also explain, at least partly, the long term positional stability of interphase chromosomes discussed above.

The strong predominance of right-handed chromosome gyres over left-handed ones is a novel finding that is at odds with previous studies in which the direction of polytene chromosome windings was investigated (7, 23). This discrepancy is probably traceable to the complexity of folding, which makes it extremely difficult to follow the chromosome paths without the aid of reliable three-dimensional modeling and cytological mapping. Furthermore, the coiling is neither absolutely right-handed nor obviously localized to particular stretches of the chromosome.

The source of the coiling asymmetry is unknown. The extensive literature on the regular spirals seen in mitotic and meiotic chromosomes gives no indication of such a chirality (26, 30), so it seems unlikely that our finding can be explained as a vestige of mitotic coiling. It could arise from some chiral aspect of the association between the chromonemata making up the polytene chromosome, which, conceivably, may originate in the right-handed DNA duplex itself. A more speculative possibility is that some of the positive helical torsion engendered by unwinding DNA, e.g., during replication, can be partitioned into higher levels of chromosome folding where it is resistant to full relaxation.

The present results do not reveal any precise long range configurations of chromosomes. More exactly, the data show that no pair of loci more than one or two cytological divisions apart is positioned close together in a large fraction of the nuclei examined. This result differs significantly from our preliminary account (27), where we had suggested the existence of specific chromosomal loops extending over as many as five cytological divisions. It now seems likely that such long range contacts coincide in only a small percentage of nuclei. The apparent conclusion is that the precise geometry of a salivary gland chromosome is not determined, and specific pairwise interactions between widely spaced genetic loci are not obligatory. More complicated combinatorial schemes, with different but specific interactions between multiple loci, have not been addressed in this study; ectopic fibers, for example, may connect sites in this way.

There remain a number of alternative explanations that are consistent with both our data and the possibility of determinate structural interactions between genetic loci. For instance, specific interactions may exist in distinct subpopulations of the gland's cells and/or in particular cell positions in the gland. There is some evidence for heterogeneity in cell type within the salivary gland (33). Consequently, the wide variation seen between nuclei may not be due to random folding but to cell type–specific differences. We have not found any obviously related subsets among the intradistance plots (see Results), but a multivariate statistical analysis is being initiated to examine this point further. Another arguable possibility is that a particular chromosome configuration is only important during the diploid or early polytene stages of the gland's development, and when we look at it, it may no longer be constrained, even though the grosser organizational motifs are retained.

These alternative explanations imply a degree of folding complexity that will make the further study of chromosome geometry correspondingly more laborious. It will be recognized, for example, that if chromosome configurations, although specific, vary from one set of cells to the next, then a direct investigation of their functional significance and the mechanisms by which they are established may be very difficult. Likewise, if specific chromosomal interactions occur early in gland development but are transient, it may be necessary to determine the three-dimensional structure of many nuclei from many time points in the gland's early development, including diploid stages; this is a formidable task. Examination of these possibilities will require the development of new methods that allow the rapid assessment of chromosome structures in many nuclei and/or in the same few cells from many samples.

The similarity between nuclei with split chromocenters and those with intact ones suggests that organizational rules such as chromosome domain separation and specific chromosome–nuclear envelope contacts are independent of gross chromosome placement within the nucleus. One implication, for example, is that the nuclear envelope structure(s) to which the specific intercalary heterochromatin loci and centromeric regions apparently attach is probably not uniquely configured relative to these sites, i.e., each particular chromosome attachment locus does not have a unique position on the nuclear envelope. Thus, it is unlikely that such interactions could contribute to a single defined geometry for each chromosome. Second, the preservation of domain boundaries in these nuclei strongly supports the notion that a direct physical impedence between chromosomal regions is responsible for their separation rather than some specific scaffolding scheme. Similarly, these nuclei provide prima facie evidence against obligatory pairwise interactions between loci on different chromosomes.

Several projects in progress in the lab will bear on the

interpretation of the present results. A large number of nuclei are being reconstructed from a single, physically sectioned salivary gland to determine whether any organizational features vary in a regular fashion from one region of the gland to another. Nuclei with ring and inverted chromosomes are also under investigation. Finally, we are examining several other larval tissues with polytene nuclei to learn which packaging motifs are tissue specific and which represent general properties of polytene nuclei.

We thank Andrew Belmont, David Agard, and Elizabeth Blackburn for critical readings of the manuscript.

This work was funded by National Institutes of Health grant GM25101 to J. W. Sedat. M. Hochstrasser is supported by a National Science Foundation predoctoral fellowship; Y. Gruenbaum is the recipient of an American Cancer Society fellowship, and M. Saumweber was supported by a postdoctoral fellowship from the Deutsche Forschungsgemeinschaft.

Received for publication 19 June 1985.

References

1. Agard, D. A., and J. W. Sedat. 1983. Three-dimensional architecture of a polytene nucleus. *Nature (Lond.).* 302:676–681.

2. Appels, R., D. M. Steffensen, and S. Craig. 1979. A new method for mapping the three-dimensional distribution of DNA sequences in nuclei. *Exp. Cell Res.* 124:436–441.

3. Ashburner, M. 1972. Puffing patterns in Drosophila melanogaster and related species. *In* Developmental Studies on Giant Chromosomes. Results and Problems in Cell Differentiation. W. Beermann, editor. Springer Verlag, Berlin. 101–151.

4. Avivi, L., and M. Feldman. 1980. Arrangement of chromosomes in the interphase nucleus of plants. *Hum. Genet.* 55:281–295.

5. Barr, H. J., and J. R. Ellison. 1972. Ectopic pairing of chromosome regions containing chemically similar DNA. *Chromosoma (Berl.).* 39:53–61.

6. Becker, H. J. 1969. The influence of heterochromatin, inversion heterozygosity and somatic pairing on x-ray induced mitotic recombination in Drosophila melanogaster. *Mol. & Gen. Genet.* 105:203–218.

7. Beermann, W. 1962. Riesenchromosomen. *Protoplasmatologia.* VI/C:1–161.

8. Bennett, M. D. 1983. Nucleotypic basis of the spatial ordering of chromosomes in eukaryotes and the implications of the order for genome evolution and phenotypic variation. *In* Genome Evolution. G. A. Dover and R. B. Flavell, editors. Academic Press, Inc., New York. 239–261.

9. Braun, W. 1983. Representation of short and long-range handedness in protein structures by signed distance maps. *J. Mol. Biol.* 163:613–621.

10. Bridges, C. B. 1935. Salivary chromosome maps. *J. Hered.* 26:60–64.

11. Burgoyne, L. A., M. A. Wagar, and M. R. Atkinson. 1971. Calcium dependent priming of DNA synthesis in isolated rat liver nuclei. *Biochem. Biophys. Res. Commun.* 39:254–259.

12. Coates, D. J., and D. Smith. 1984. The spatial distribution of chromosomes in metaphase neuroblast cells from subspecific F1 hybrids of the grasshopper Caledia captiva. *Chromosoma (Berl.).* 90:338–348.

13. Comings, D. E. 1980. Arrangement of chromatin in the nucleus. *Hum. Genet.* 53:131–143.

14. Ellison, J. R., and G. C. Howard. 1981. Non-random position of the A-T rich DNA sequences in early embryos of Drosophila virilis. *Chromosoma (Berl.).* 83:555–561.

15. Foe, V. E., and B. M. Alberts. 1985. Reversible chromosome condensation induced in Drosophila embryos by anoxia: visualization of interphase nuclear organization. *J. Cell Biol.* 100:1623–1636.

16. Fussell, C. P. 1975. The position of interphase chromosomes and late replicating DNA in centromere and telomere regions of Allium cepa L. *Chromosoma (Berl.).* 50:201–210.

17. Gay, H. 1956. Nucleocytoplasmic relations in Drosophila. *Cold Spring Harbor Symp. Quant. Biol.* 21:257–269.

18. Gruenbaum, Y., M. Hochstrasser, D. Mathog, H. Saumweber, D. A. Agard, and J. W. Sedat. 1984. Spatial organization of the Drosophila nucleus: a three-dimensional cytogenetic study. *J. Cell Sci.* (Suppl. 1):223–234.

19. Halfer, C., and C. Barigozzi. 1973. Prophase synapsis in somatic cells of Drosophila melanogaster. *In* Chromosomes Today. A. de la Chapelle and M. Sorsa, editors. Elsevier North-Holland Biomedical Press, Amsterdam. 4:181–186.

20. Hammond, M. P., and C. D. Laird. 1985. Control of DNA replication and spatial distribution of defined DNA sequences in salivary gland cells of Drosophila melanogaster. *Chromosoma (Berl.).* 91:279–286.

21. Hancock, R., and T. Boulikas. 1982. Functional organization in the nucleus. *Int. Rev. Cytol.* 79:165–214.

22. Herreros, B., and F. Gianelli. 1967. Spatial distribution of old and new chromatid sub-units and frequency of chromatid exchanges in induced human lymphocyte endoreduplications. *Nature (Lond.).* 216:286–288.

23. Koller, P. C. 1935. The internal mechanics of the chromosomes. IV. Pairing and coiling in salivary gland nuclei of Drosophila. *Proc. R. Soc. Lond. B Biol. Sci.* 118:371–396.

24. Lefevre, G. 1976. A photographic representation and interpretation of the polytene chromosomes of Drosophila melanogaster salivary glands. *In* The Genetics and Biology of Drosophila. Volume 1A. M. Ashburner and E. Novitski, editors. Academic Press, Inc., New York. 31–66.

25. Lifschytz, E., and D. Haravan. 1982. Heterochromatin markers: arrangement of obligatory heterochromatin, histone genes, and multisite gene families in the interphase nucleus of D. melanogaster. *Chromosoma (Berl.).* 86:443–455.

26. Manton, I. 1950. The spiral structure of chromosomes. *Biol. Rev.* 1:486–508.

27. Mathog, D., M. Hochstrasser, Y. Gruenbaum, H. Saumweber, and J. Sedat. 1984. Characteristic folding pattern of the polytene chromosomes in Drosophila salivary gland nuclei. *Nature (Lond.).* 308:414–421.

28. Mathog, D. 1985. Light microscope based analysis of three-dimensional structure: applications to the study of Drosophila salivary gland nuclei. II. Algorithms for model analysis. *J. Microsc.* 137:254–275.

29. Mathog, D., M. Hochstrasser, and J. W. Sedat. 1985. Light microscope based analysis of three-dimensional structure: applications to the study of Drosophila salivary gland nuclei. I. Data collection and analysis. *J. Microsc.* 137:241–253.

30. Ohnuki, Y. 1968. Structure of chromosomes. I. Morphological studies of the spiral structure of human somatic chromosomes. *Chromosoma (Berl.).* 25:402–428.

31. Pearson, M. J. 1974. Polyteny and the functional significance of the polytene cell cycle. *J. Cell Sci.* 15:457–479.

32. Pera, F., and H. G. Schwarzacher. 1970. Lokalisation der heterochromatischen Chromosomen von Microtus agrestis in Interphase und Mitose. *Cytobiologie.* 2:188–199.

33. Probeck, H., and L. Rensing. 1974. Cellular patterns of differing circadian rhythms and levels of RNA synthesis in Drosophila salivary glands. *Cell Differ.* 2:337–345.

34. Quick, P. 1980. Junctions of polytene chromosomes and the inner nuclear membrane. *Experientia.* 36:456–457.

35. Rabl, C. 1885. Uber Zelltheilung. *Morph. Jb.* 10:214–330.

36. Rossman, M. G., and A. J. Liljas. 1974. Recognition of structural domains in globular proteins. *J. Mol. Biol.* 85:177–181.

37. Shield, G., and J. H. Sang. 1970. Characteristics of five cell types appearing during in vitro culture of embryonic material from Drosophila melanogaster. *J. Embryol. Exp. Morph.* 23:53–69.

38. Sonnenblick, B. P. 1950. The early embryology of Drosophila melanogaster. *In* Biology of Drosophila. M. Demerec, editor. J. Wiley & Sons, New York. 62–167.

39. Sperling, K., and E-K. Luedke. 1981. Arrangement of prematurely condensed chromosomes in cultured cells and lymphocytes of the Indian muntjac. *Chromosoma (Berl.).* 83:541–553.

40. Spofford, J. B. 1976. Position effect variegation in Drosophila. *In* The Genetics and Biology of Drosophila. Volume 1C. M. Ashburner and E. Novitski, editors. Academic Press, Inc., New York. 955–1018.

41. Steffenson, D. M. 1977. Chromosome architecture and the interphase nucleus: data and theory on the mechanisms of differentiation and determination. *In* Chromosomes Today. Volume 6. A. de la Chapelle and M. Sorsa, editors. Elsevier North-Holland Biomedical Press, Amsterdam. 247–253.

42. Sved, J. A. 1976. Hybrid dysgenesis in Drosophila melanogaster: a possible explanation in terms of spatial organization of chromosomes. *Aust. J. Biol. Sci.* 29:375–388.

43. Zhimulev, I. F., V. F. Semeshin, V. A. Kulichkov, and E. S. Belyaeva. 1982. Intercalary heterochromatin in Drosophila. I. Localization and general characteristics. *Chromosoma (Berl.).* 87:197–228.

44. Zorn, C., C. Cremer, T. Cremer, and J. Zimmer. 1979. Unscheduled DNA synthesis after partial U.V.-irradiation of the cell nucleus. Distribution in interphase and metaphase. *Exp. Cell Res.* 124:111–119.